Металлофиз. новейшие технол. / *Metallofiz. Noveishie Tekhnol.*
2018, т. 40, № 3, сс. 397–409 / DOI: 10.15407/mfint.40.03.0397
Оттиски доступны непосредственно от издателя
Фотокопирование разрешено только
в соответствии с лицензией

Напечатано в Украине.

PHYSICS OF STRENGTH AND PLASTICITY

PACS numbers: 61.05.cp, 62.20.Qp, 62.23.Pq, 68.37.Hk, 81.16.Rf, 81.40.Pq, 81.65.Kn

Effect of Nano-TiO_2 Particles on Wear and Corrosion Behaviour of AA6063 Surface Composite Fabricated by Friction Stir Processing

D. Muthukrishnan, A. N. Balaji, and G. R. Raghav

K.L.N. College of Engineering, Department of Mechanical Engineering, 630612 Pottapalayam, Sivagangai District, Tamil Nadu, India

In this investigation, the effect of nano-TiO_2 particles on wear and corrosion behaviour of AA6063 surface nanocomposites produced *via* friction stir processing (FSP) was studied. Microstructure analysis of fabricated surface nanocomposites was done with scanning electron microscope and found that TiO_2 nanoparticles are uniformly dispersed in the stir zone. The surface nanocomposites were characterized by hardness, wear and corrosion tests. The results revealed that the microhardness increases due to the presence of hard TiO_2 nanoparticles than as AA6063 alloy. The FSPed surface nanocomposites exhibited low frictional coefficient, excellent wear resistance and adequate corrosion resistance at 40 mm/min and as compared to that of the as cast alloy.

Key words: AA6063 alloy, TiO_2 nanoparticles, friction stir processing, surface nanocomposites, microstructure, microhardness, wear behaviour, corrosion behaviour.

Досліджено вплив наночастинок TiO_2 на характер зношування та корозії поверхневих нанокомпозитів стопу AA6063, одержаних за допомогою оброблення тертям з перемішуванням. Проведено аналізу одержаних поверхневих нанокомпозитів методою сканувальної електронної мікроскопії та встановлено, що наночастинки TiO_2 рівномірно розподілені в зоні перемішування. Для характеризації поверхневих нанокомпозитів було використано випробування на твердість, зносостійкість і корозійну стійкість. Показано, що мікротвердість підвищується у порівнянні зі стопом AA6063 завдяки наявності наночастинок TiO_2. Оброблені методою тертя з

Corresponding author: A. N. Balaji
E-mail: balajime@yahoo.com

Citation: D. Muthukrishnan, A. N. Balaji, and G. R. Raghav, Effect of Nano-TiO_2 Particles on Wear and Corrosion Behaviour of AA6063 Surface Composite Fabricated by Friction Stir Processing, *Metallofiz. Noveishie Tekhnol.*, **40**, No. 3: 397–409 (2018), DOI: 10.15407/mfint.40.03.0397.

перемішуванням поверхневі нанокомпозити мають низький коефіцієнт тертя, відмінну зносостійкість й адекватну корозійну стійкість при 40 мм/хв. у порівнянні зі стопом у литому стані.

Ключові слова: стоп AA6063, наночастинки TiO_2, оброблення фрикційним перемішуванням, поверхневі нанокомпозити, мікроструктура, мікротвердість, характеристики зношування, корозійні властивості.

Исследовано влияние наночастиц TiO_2 на характер износа и коррозии поверхностных нанокомпозитов сплава AA6063, полученных с помощью обработки трением с перемешиванием. Проведён анализ поверхностных нанокомпозитов методом сканирующей электронной микроскопии и показано, что наночастицы TiO_2 равномерно распределены в зоне перемешивания. Для характеризации поверхностных нанокомпозитов были использованы испытания на твёрдость, износостойкость и коррозионную стойкость. Показано, что микротвёрдость повышается по сравнению со сплавом AA6063 благодаря наличию наночастиц TiO_2. Обработанные методом трения с перемешиванием поверхностные нанокомпозиты обладают низким коэффициентом трения, отменной износостойкостью и адекватной коррозионной стойкостью при 40 мм/мин по сравнению со сплавом в литом состоянии.

Ключевые слова: сплав AA6063, наночастицы TiO_2, обработка фрикционным перемешиванием, поверхностные нанокомпозиты, микроструктура, микротвёрдость, характеристики износа, коррозионные свойства.

(Received November 17, 2017)

1. INTRODUCTION

The cast aluminium alloy AA6063, containing Si and Mg as its major alloying element, is mainly used in a variety of structural, automotive, aerospace and engineering applications due to their high strength to weight ratio, excellent casting characteristics, low coefficient of thermal expansion, high thermal conductivity, good mechanical properties and low cost. However, its wider application is limited because of its inferior hardness, wear and corrosion properties. In recent years, the further improvement in hardness, wear and corrosion properties of cast AA6063 alloy would be achieved by several techniques such as incorporating ceramic particles such as Al_2O_3, SiC and so on as reinforcement material in AA6063 alloy, decreasing the particle size of reinforcements to nanometric scale and surface composite fabrication [1]. Various studies have shown that particulate reinforced aluminium matrix nanocomposites exhibit excellent wear and corrosion characteristics and improved thermal and mechanical properties as compared to monolithic materials [2–4]. Nowadays, the surface composite fabrication technique has attracted more attentions by several researchers. There are several techniques for fabricating surface aluminium matrix

nanocomposite such as plasma spraying, high-energy electron beam irradiation, high-energy laser melt treatment, casting and friction stir processing (FSP) [5, 6]. Except FSP, all of the other techniques are based on liquid phase processing at higher temperatures and impossible to avoid the reaction between the reinforcements and the matrix, which forms undesirable phases [6]. In this concern, recently, eco-friendly and solid-state technique known as FSP based on friction stir welding, which is operated below melting temperature of matrix, is given more attention by researchers for the fabrication of surface composites [7].

In the FSP, a specially designed tool with high rotating speed is inserted into the metal plate and it transverses in the desired direction. During FSP, metal is subjected to high plastic deformation and high heat exposure, which result in a modified microstructure characterized by a fine and equiaxed by dynamic recrystallization. FSP is widely used for fabricating the micro/nanoparticle reinforced surface composites [7–9]. Morisada *et al.* [10] improved the hardness and thermal stability of AZ31 by dispersing multiwalled carbon nanotubes as reinforcement into the AZ31 alloy by FSP. Narmani *et al.* [11] have evaluated about the wear behaviour of AA6063/hybrid surface composite by FSP; they found that the embedment of B_4C and TiB_2 ceramic particles on the surface increased the hardness and improved the wear behaviour of composite layers in comparison with FSPed AA6063. Mishra *et al.* [12] have studied about the effect of processing parameters such as hole geometry, pattern and number of passes in the fabrication of Al–B_4C composites by incorporating B_4C particles into the 5024 Al matrix. They found that the modulus of the composite layer is almost twice that of the base metal modulus. Lakshmanan *et al.* [13] studied about the performance characteristics of AA6061/nano-B_4C metal matrix nanocomposites by using ultrasonic cavitation assisted casting process and observed that wear resistance of aluminium alloy–nano-boron carbide composites compared to the monolithic alloy very much improved. Khodabakhshi *et al.* [14] fabricated the Al–Mg nanocomposites by incorporating TiO_2 particles and found that solid-state chemical reaction between TiO_2 nanoparticles and the Al–Mg matrix led to in situ formation of Al_3Ti and MgO nanoparticles.

The previous studies reveal that most of the researchers concentrated on fabricating aluminium matrix micro/nanocomposites *via* FSP using the ceramic particles such as Al_2O_3, SiC, B_4C as reinforcement [16–18]. However, to the best of author's knowledge, limited information exists on their wear behaviour, no information exists on their corrosion behaviour, and there is no through work reporting the fabrication of AA6063/TiO_2 surface nanocomposites *via* FSP. TiO_2 is one of the most important used in the engineering material. This titanium based material offers high strength, good corrosion and oxidation resistance. The incorporation of nanoparticles can greatly improve the mechanical,

tribological properties and corrosion resistance, resistance of matrix material, and hence it can be used as reinforcement for fabrication of nanocomposites. Based on the above concern, the present investigation was focused on fabricating AA6063/TiO_2 surface nanocomposites *via* FSP and to study the influence of tool rotational speed on the microstructure, microhardness, wear and corrosion properties of AA6063/TiO_2 surface nanocomposites fabricated by double pass FSP.

2. MATERIALS AND METHODS

2.1. TiO_2 Particles

The micron sized (< 10 μm) TiO_2 powders were purchased (SIGMA-ALDRICH, Germany) and reduced to nanosize by employing high-energy ball mill (Fritsch pulverisette, Germany).

2.2. Friction Stir Processing

As cast received, AA6063 billet was cut by wire cut Electrical Discharge Machining (EDM) machine with dimensions of 100 mm length, 50 mm width, 6 mm depth used as substrate material. The nominal alloy composition was Al–6.89 Si–0.42 Mg–0.007 Mn–0.014 Cu–0.13 Fe–0.03 Zn–0.16 Ti–0.003 Cr–0.007 Ni (% wt.). TiO_2 nanoparticles of 36.85 nm size were used as reinforcement. Then, TiO_2 particles were filled in the groove (2 mm depth, 3 mm width), which was machined in the middle of the AA6063 specimens. The schematic sketch of the aluminium alloy specimen for FSP is shown in Fig. 1. The FSP tool made of hardened En-13, which had a columnar shape with a shoulder (∅ 18 mm) and terminating in square pin (∅ 6 mm, pin height 3 mm).The geometry and dimensions of the FSP tool is shown in Fig. 2. The FSP machine used here was a modified vertical milling machine.

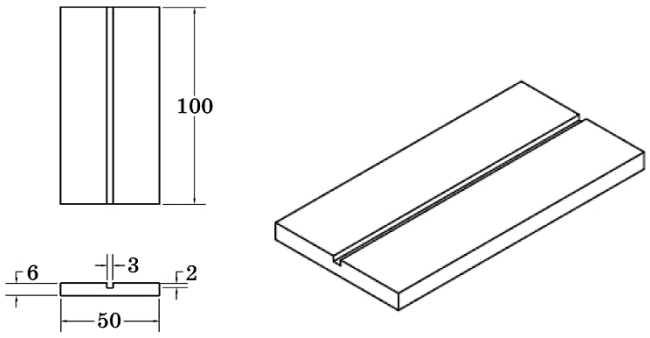

Fig. 1. Schematic diagram of aluminium alloy specimen for FSP.

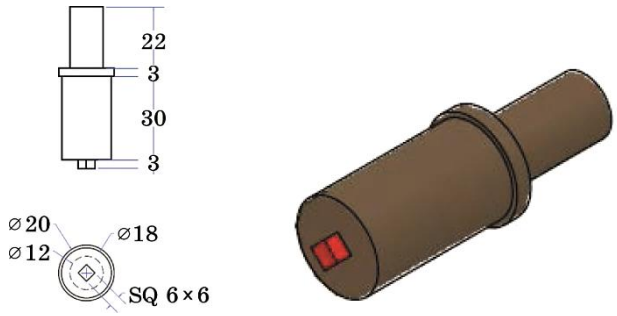

Fig. 2. Geometry and dimensions (mm) of the FSP tool.

During processing, the scattering of powder from the groove is prevented by capping pass, which was done by pin less tool. The processing parameters used for capping pass were 800 rpm tool rotation rate, 25 mm/min tool traverse speed and zero tool tilt angle. The three different tool rotation rates (900 rpm, 1200 rpm, and 1600 rpm) and constant traverse speed (40 mm/min) were set for the stirring processes. The plates were subjected to two passes for each parameter, and plates were rotated by 180° to obtain better powder distribution and reduce the agglomeration of powders in the advancing side. The FSPed specimens at 900 rpm, 1200 rpm, and 1600 rpm are shown in Fig. 3.

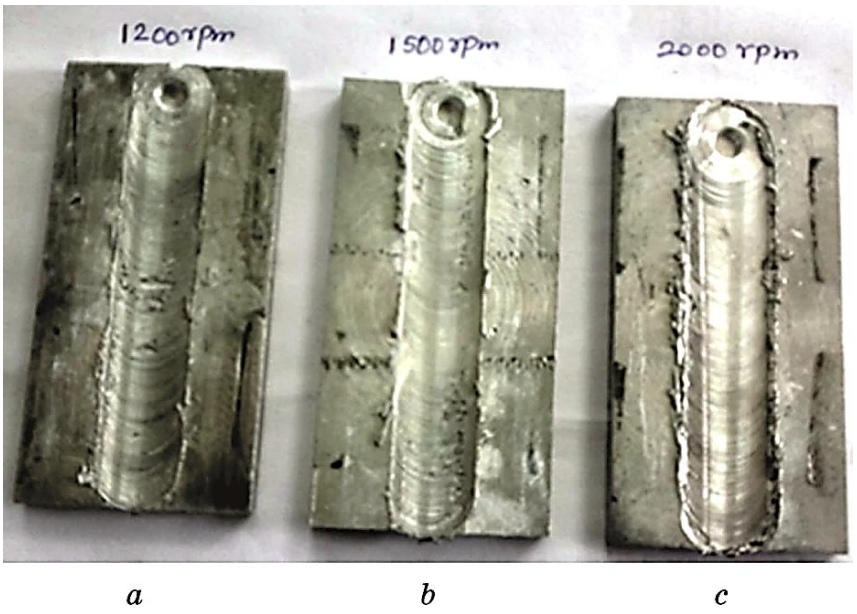

Fig. 3. FSPed specimens at: 900 rpm (*a*), 1200 rpm (*b*), 1600 rpm (*c*).

2.3. Characterization Techniques

The surface morphology of the processed samples was characterized using scanning electron microscope (SEM) (Hitachi SUI 510, Japan operating in secondary electron mode, at an accelerating voltage of 10 kV, emission current of 96 μA).

The microhardness of the surface composites were evaluated by using Vickers microhardness tester under a load of 100 kgf load and 0.5 mm steel ball indenter with a dwell time of 10 s. A reported test measurement represents the average of 10 indentation values.

A pin on disc type wear monitor (WINDUCOM) with data acquisition system was used to evaluate the wear behaviour of processed samples against hardened ground steel (En-31) disc having hardness of RC60 and surface roughness (R_a) 0.5 μm. The pin and the disc were abraded against carbide polishing papers, washed with acetone, and dried before each sliding test to ensure that the tests were carried out under nominally dry sliding conditions. The system had maximum loading capacity of 200 N. The sample wear pin dimension is 25×3×3 mm. The applying load is 9.82 N, rotation speed of the disc is 500 rpm, the diameter of the disc is 100 mm and duration is 60 min.

Potentiometric polarization measurements were carried out by using Electrochemical workstation consisting of platinum wire electrode, Ag/AgCl reference electrode, and friction stir processed specimen taken in turn as working electrode. All the electrochemical tests were performed at 25°C with 5% NaCl solution as electrolyte. A polarization phenomenon of the base metal and FSPed specimen was studied at a scan rate of 5 mV/s. Before taking measurements, all the specimens were immersed in the 5% NaCl solution for one hour to be stabilized. The open circuit potential was measured after reaching a steady state, and then the polarization measurements were done. The corrosion potential (E_{Corr}) and the corrosion current density (I_{Corr}) were calculated from the intersection of the cathodic and anodic Tafel extrapolation method.

3. RESULTS AND DISCUSSIONS

3.1. Microstructure Analysis

The structural features of TiO_2 were studied using XRD. Figure 4 shows the strong Bragg reflections (JCPDS.No.75-0424) were seen in the XRD, which correspond to the reflection of TiO_2. The XRD patterns of the samples exhibit the characteristic peak at $2\theta = 27°$, which corresponds to the (110) plane of TiO_2 thereby confirming the presence of TiO_2. Figure 5, *a* shows the SEM micrograph of base metal AA6063. From Figure 5, *a*, it is known that AA6063 consists of white coloured matrix of alpha solid solution dendrites and black coloured second phase silicon rich eutectic

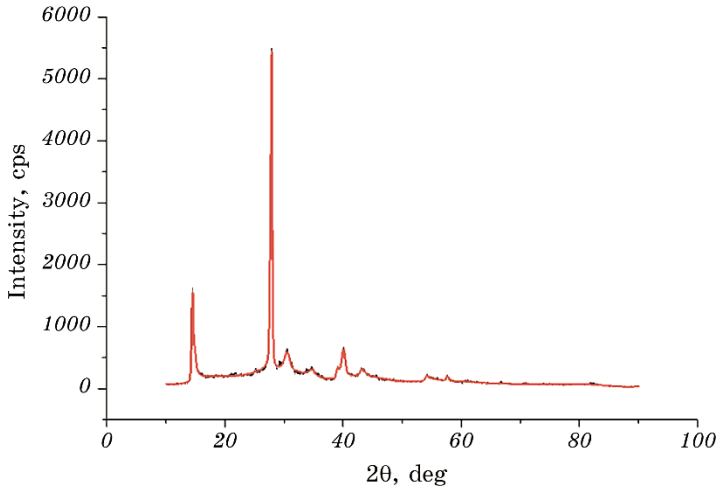

Fig. 4. XRD pattern of nano-TiO_2.

coarse structure. It can be seen that base metal consists of grains size varying between 30–45 μm. The processed specimens have stir zone, which was characterized by fine and equiaxed grain structure due to plastic deformation and high frictional heat generation.

Figure 5, *b*–*d* shows the metallographs of FSPed specimens under different rotational speeds and constant traverse speed. It is evident that FSPed specimen at 1200 rpm shows better particle distribution

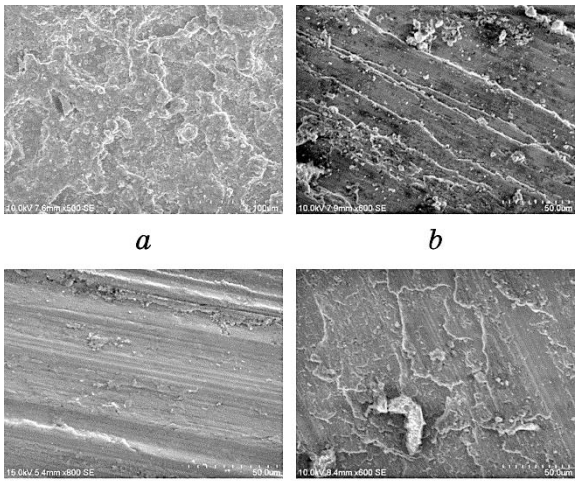

Fig. 5. SEM micrographs of: base metal (*a*), FSPed at 900 rpm (*b*), FSPed at 1200 rpm (*c*), FSPed at 1600 rpm (*d*).

and, in that, there was no agglomeration of nanoparticles (TiO_2) and finer grain size refinement, which is caused due to generation of high heat energy, and there is enough time to material flow along the substrate. These effects were attributed by high rotational speed, which causes new nucleation sites leading to grain size reduction. The traverse speed is maintained constant at 40 mm/min for different rotation speeds to avoid the lower heat input due to short duration of the process. To avoid the pinning effect of the ceramic particles and agglomeration of the particles, constant traverse speed is maintained, and good bonding is achieved with substrate material. Increasing either tool rotation rate or rotation rate/traverse speed ratio leads to elimination of the banded structure [4, 18]. Therefore, higher tool rotation rate intensifies frictional heating and stirring, which creates a higher temperature in the stirred zone and subsequently more proper mixing of material, which leads to uniform dispersement of nanoparticles.

3.2. Microhardness Behaviour

The wear behaviour of material relates inversely with the hardness, as hardness increases, the wear of material decreases. It is an important parameter for the tribological behaviour of materials and is considered before conducting wear tests. Figure 6 depicts the microhardness readings of the specimens FSPed with different rotational speeds (900 rpm, 1200 rpm, and 1600 rpm) at a constant traverse speed of 40 mm/min. It can be observed that increasing the rotational speed tends to reduce the microhardness values. This is due to improved dynamic recrystallization, which is caused by higher stirring action of the tool with pin. It also evident from the figure that the specimens processed with rota-

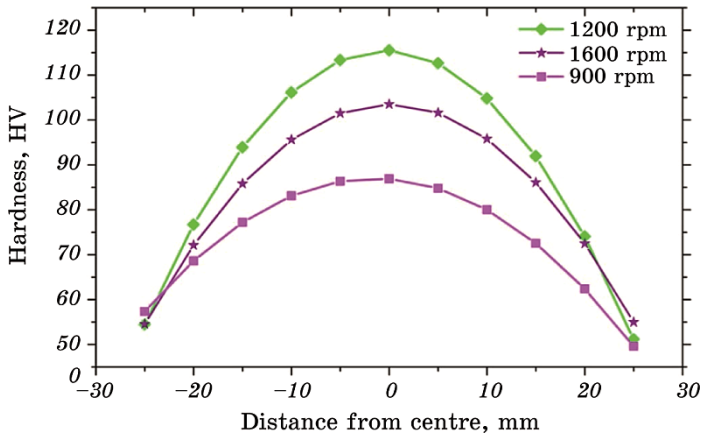

Fig. 6. Hardness profiles.

tional speed of 1200 rpm have higher hardness than the specimens processed with 1600 rpm and 900 rpm do. The specimen FSPed at 1200 rpm has uniform distribution of TiO_2 particles, *i.e.* average spacing between the particles was very good. It is revealed that, as the rotational speed increases, the microhardness also increases that is due to the increase in heat input that causes easier and more intense stirring action of the rotating pin resulting in better dispersion of reinforcement particles thus increasing the microhardness [20–22]. Low annealing effect of heat input increases the microhardness behaviour under high rotational speed. In addition, further improving the rotational speed tends to decrease the microhardness values in the surface composites matrix. The reason behind this that generation of high input due to high rotational speed makes the matrix softening which reduces the microhardness. The softening of matrix resulted in coarsening and/or dissolution of strengthening precipitates in the aluminium matrix, which occurs especially in heat treatable aluminium alloys.

3.3. Wear Evaluation

A comparison of wear behaviour of processed zone of AA6063/TiO_2 composite at different speeds (900 rpm, 1200 rpm, 1600 rpm) and as received AA6063 is shown in Fig. 7. From Figure 7, it is known that

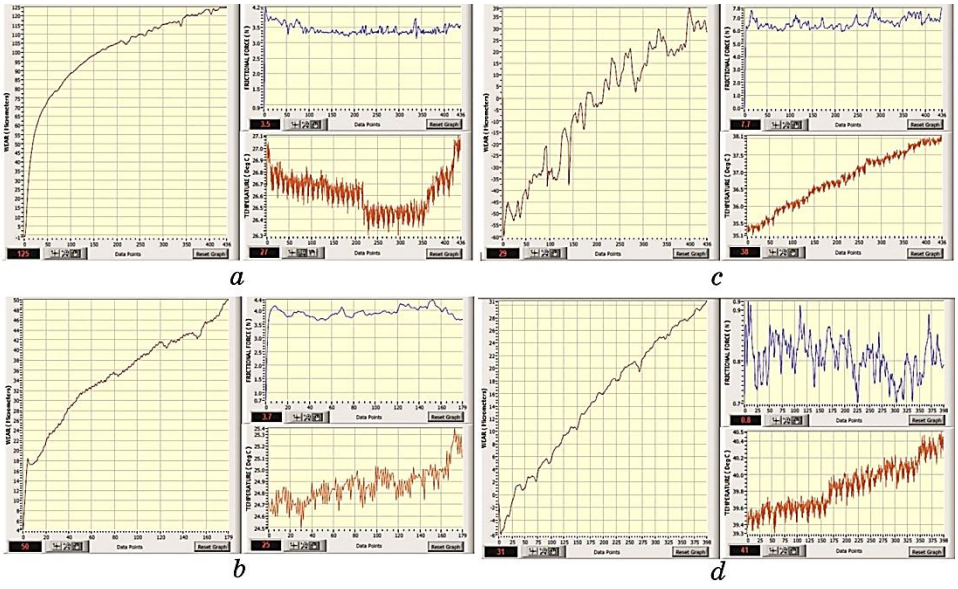

Fig. 7. Wear rate curves for: A356 (*a*), FSPed at 900 rpm (*b*), FSPed at 1200 rpm (*c*), FSPed at 1600 rpm (*d*).

TABLE 1. Wear rate.

No.	Specimen	Wear, μm	Frictional force, N
1	AA6063	125	3.5
2	AA6063/TiO_2 FSPed at 900 rpm	50	3.7
3	AA6063/TiO_2 FSPed at 1200 rpm	29	7.7
4	AA6063/TiO_2 FSPed at 1600 rpm	31	0.8

FSPed specimen at 1200 rpm exhibits lower wear rate (29 μm) and high frictional force value, *i.e.* (7.7 N) when compared with the FSPed specimens at (900 and 1600 rpm) and base metal (as received AA6063) respectively. It is clearly known that dispersion of fine TiO_2 particles along the substrate acts as hard ceramic phase in base metal improves the wear resistance. It is well-known fact that hardness improvement is inversely proportional to wear rate.

Table 1 provides the details of wear variation of as cast AA6063 and FSPed specimen, *i.e.* surface composite layer produced at rotational speed 1200 rpm and traverse speed of 40 mm/min respectively. To identify the genesis of wear, scanning electron microscopy of the worn surfaces was undertaken and is shown in Fig. 8. It was known that tangential and normal loads are transmitted through contact regions due to ploughing and adhesive wear mechanism. From Figure 8, *a*, it is clear that the worn surface of as AA6063 alloy consists of wide continuous parallel grooves.

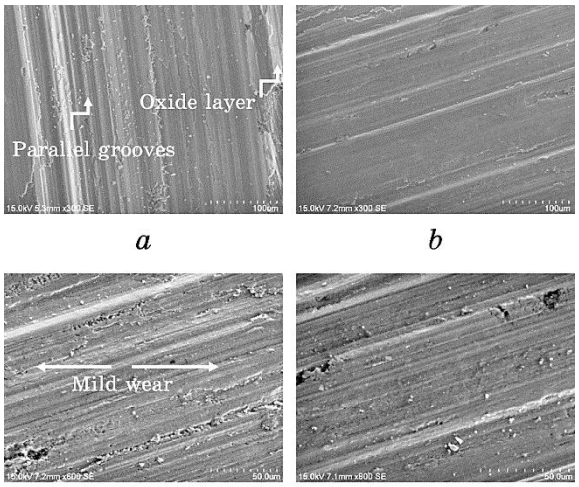

Fig. 8. SEM micrographs of worn surfaces: base metal (*a*), FSPed specimen at 900 rpm (*b*), FSPed specimen at 1200 rpm (*c*), FSPed specimen at 1600 rpm (*d*).

This indicates deeper penetration of the asperities of the harder disc and removal of more material from the contact surface of the wear pin, and hence, severe wear mode was observed in as AA6063 alloy. It also shows that, in the absence of grain refinement there was a larger amount of fracture. The dislodging of the surfaces and removal of the material along the grain boundary lead to delamination wear. For processed AA6063 alloy with nanoparticles, the worn surface shown in Fig. 8, *b*–*d* displays fine grooves and with few small dimples when compared to the as cast alloy as seen in Fig. 8, *a*. The reduction in wear of AA6063 alloy could be due to the fact that the addition of refiner leads to decrease in the grain size and formation of more number of grain boundaries.

Such structural changes lead to the improvement in toughness and strength of the alloy owing to reduced wear rate. In the grain-refined alloy, there was no crack formation on the worn surface and the wear mode observed was abrasive as clearly evident from Fig. 8, *c*. The abrasive wear occurs because of the sliding of hard disc against soft pin surface. The disc digs into the pin surface and ploughs a series of continuous parallel grooves (two-body wear). Abrasive wear also occurs when hard silicon particles are introduced between the two sliding surfaces.

3.4. Corrosion Behaviour

For the corrosion test, the specimen processed at 1200 rpm that yields higher hardness value (110 *HV*), and lower wear rate (29 μm) is taken to compare with base metal. The polarization curves for AA6063 alloy base metal and FSPed specimen at 1200 rpm are as shown in Fig. 9. The

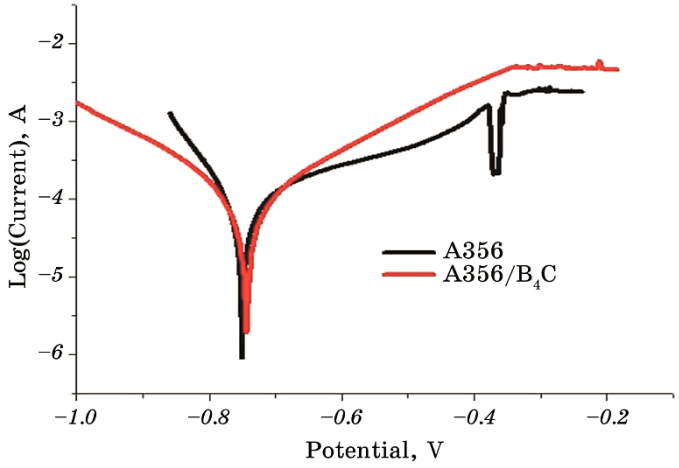

Fig. 9. Potentiodynamic polarization curves.

corrosion potential (E_{Corr}) and the corrosion current density (I_{Corr}) were calculated from the intersection of the cathodic and anodic Tafel extrapolation method. The E_{Corr} and I_{Corr} of base A356 alloy are obtained as −751.17 mV and 12.270 μA, and for the FSPed specimen at 1200 rpm, are obtained as −744.05 mV and 9.92 μA. The E_{Corr} of the base metal is more than that of FSPed specimen with TiO_2 particles that indicates the increase in resistance to corrosion of FSPed specimen when compared with base metal.

4. CONCLUSIONS

The effect of TiO_2 particles on microstructure, microhardness, and wear and corrosion behaviour of AA6063 surface composite fabricated by FSP was investigated and the following conclusions were obtained.

The microstructures studies indicated that good bonding of TiO_2 with AA6063 substrate generated at 1200 rpm when comparing with base metal and FSPed specimens at 900 and 1600 rpm.

The microhardness values were found for AA6063 and AA6063/TiO_2 at 1200 rpm surface composite were 58 *HV* and 120 *HV*. The increase of hardness value is due to presence of nanoparticles and significant modification due to FSP.

The wear rate of FSPed specimen at 1200 rpm is 29 μm that is very lower value when compared with that of as received base metal (125 μm). The sudden reduction in wear rate can be achieved as particles act as hard phase and obstacles to wear producing factors.

Due to the presence of TiO_2 particles, corrosion resistance increased from −0.757 mV to −0.744 mV.

REFERENCES

1. L. Karthikeyan and V. S. Senthilkumar, *Mater. Des.*, **32**: 3085 (2011).
2. B. Zahmatkesh and M. H. Enayati, *Mater. Sci. Eng. A*, **527**: 6734 (2010).
3. Y. Mazaheri, F. Karimzadeh, and M. H. Enayati, *J. Mater. Process. Technol.*, **211**: 1614 (2011).
4. G. M. Reddy and K. S. Rao, *Trans. Indian Inst. Metals*, **63**: 793 (2010).
5. Z. Y. Ma, *Metall. Mater. Trans. A*, **39**: 642 (2008).
6. R. S. Mishra and N. Kumar, *Friction Stir Welding and Processing: Science and Engineering* (London: Springer: 2014).
7. P. B. Berbon, W. H. Bingel, R. S. Mishra, C. C. Bampton, and M. W. Mahoney, *Scr. Mater.*, **44**: 61 (2001).
8. A. D. Ehab, M. E. Magdy, and S. Mahmoud, *Mater. Des.*, **31**: 1231 (2010).
9. S. R. Sharma, Z. Y. Ma, and R. S. Mishra, *Scr. Mater.*, **51**: 237 (2004).
10. Y. Morisada, H. Fujii, T. Nagaoka, and M. Fukusumi, *Mater. Sci. Eng. A*, **419**: 344 (2006).
11. M. Narimani, B. Lotfi, and Z. Sadeghian, *Surf. Coat. Technol.*, **285**: 1 (2016).
12. R. S. Mishra, P. S. De, and N. Kumar, *Friction Stir Welding and Processing:*

Science and Engineering (Springer: 2014).
13. P. Lakshmanan, K. Kalaichelvan, and T. Sornakumar, *Mater. Manufact. Processes*, **31**: 1275 (2016).
14. F. Khodabakhshi, A. Simchi, A. H. Kokabi, M. Sadeghahmadi, and A. P. Gerlich, *Mater. Sci. Technol.*, **31**: 4 (2015).
15. N. Yuvaraj, S. Aravindan, and Vipin, *J. Mater.Res. Technol.*, **4**: 398 (2015).
16. R. Srinivasu, A. S. Rao, G. M. Reddy, and K. S. Rao, *Def. Technol.*, **11**: 140 (2015).
17. L. Chen, H. Konishi, A. Fehrenbacher, and C. Ma, *Scr. Mater.*, **67**: 29 (2012).
18. A. Devaraju, A. Kumar, A. Kumaraswamy, and B. Kotiveerachari, *Mater. Des.*, **51**: 331 (2013).
19. S. K. Singh, R. J. Immanuel, S. Babu, and S. K. Panigrahi, *J. Mater. Process. Technol.*, **236**: 252 (2016).
20. L. S. Raju and A. Kumar, *Def. Technol.*, **10**: 375 (2014).
21. D. G. Mallapur, K. R. Udupa, and S. A. Kori, *Tribology—Materials, Surfaces Interfaces*, **5**: 34 (2013).
22. R. Harichandran and N. Selvakumar, *Arch. Civ. Mech. Eng.*, **16**: 147 (2016).